npj | 2D Materials and Applications

www.nature.com/npj2dmaterials

ARTICLE OPEN

Check for updates

# Postsynthetic treatment of nickel–iron layered double hydroxides for the optimum catalysis of the oxygen evolution reaction

Daire Tyndall[1,2], Sonia Jaskaniec[1,2], Brian Shortall[2,3], Ahin Roy[1,2], Lee Gannon[2,3], Katie O'Neill[1,2], Michelle P. Browne[1,2], João Coelho[1,2,4], Cormac McGuinness[2,3], Georg S. Duesberg[1,2,5] and Valeria Nicolosi[1,2,6]✉

Nickel–iron-layered double hydroxide (NiFe LDH) platelets with high morphological regularity and submicrometre lateral dimensions were synthesized using a homogeneous precipitation technique for highly efficient catalysis of the oxygen evolution reaction (OER). Considering edge sites are the point of activity, efforts were made to control platelet size within the synthesized dispersions. The goal is to controllably isolate and characterize size-reduced NiFe LDH particles. Synthetic approaches for size control of NiFe LDH platelets have not been transferable based on published work with other LDH materials and for that reason, we instead use postsynthetic treatment techniques to improve edge-site density. In the end, size-reduced NiFe LDH/single-wall carbon nanotube (SWCNT) composites allowed to further reduce the OER overpotential to 237 ± 7 mV ($<L> = 0.16 \pm 0.01$ µm, 20 wt% SWCNT), which is one of the best values reported to date. This approach as well improved the long-term activity of the catalyst in operating conditions.

*npj 2D Materials and Applications* (2021)5:73 ; https://doi.org/10.1038/s41699-021-00249-6

## INTRODUCTION

One of the most significant concerns in modern society is the imminent energy crisis, which will be faced if fossil fuels cannot be successfully replaced by some renewable and clean alternative energy source[1,2]. At the moment, $H_2$ gas seems to be a viable option, as it combusts cleanly in air and has more chemical energy per unit weight than gasoline and common battery materials[1]. Unfortunately, $H_2$ gas is not readily available in nature. The cheapest and most popular synthetic route for industrial-scale hydrogen production to date is steam reforming using natural gas[3]. A cleaner method of production can be achieved via the extraction of $H_2$ from water by electrolysis[1,2,4]. Water splitting consists of two half reactions, the hydrogen evolution reaction (HER) and oxygen evolution reaction (OER)[1,2,4]. While HER is a relatively simple process, OER is characterized by sluggish kinetics[2,4,5]. Thus, in practice, OER is observed at applied potentials higher than its predicted equilibrium potential[4]. This excess overpotential (η) renders the overall water electrolysis an energetically costly process[6,7]. To this day, water electrolysis accounts for just 4% of the world's hydrogen production because the energy cost remains high, meaning more efficient catalysis of the OER reaction is imperative[1,2,4,8]. Layered double hydroxides (LDH) are among the materials of highest interest in research today, owing to their desirable chemical and electrochemical properties, with applications in electrocatalysis,[1,2,4,9–12] as well as energy storage and drug delivery[13]. In particular, nickel–iron (NiFe) LDH is a material with impressive catalytic properties as a result of a high density of active sites whose activity is enhanced by a charge-transfer activation mechanism between the Ni and Fe metal centers[14]. Moreover, the LDH's relatively open brucite-like structure promotes also a fast diffusion of reactants and products during catalysis[9,10]. For comparison purposes, in terms of OER overpotential and stability in operating conditions, NiFe LDH outperforms competitive and more conventional catalyst materials, such as $RuO_2$ and $IrO_2$ as well as Raney Nickel (Alkaline Water Electrolysis), while also being significantly cheaper[1,2,11,15,16]. Not surprisingly, the development of synthesis routes[17,18] had lead to new and improved NiFe LDH-based catalysts, such as molecule intercalated LDH[18], nanoparticles[2,19–21] and NiFe LDH/carbon hybrids[19–21], among others[22,23]. In its pure form, NiFe LDH can comfortably produce OER overpotentials below 400 mV (@ 10 mA. $cm^{-2}$), which can be pushed to considerably lower values with various novel systems. For example, Song et al.[24] achieve 300 mV by exfoliation alone, while Gong et al.[25] demonstrate 220 mV for NiFe LDH platelets grown directly onto a carbon nanotube (CNT) binder. All of these attempts aim at increasing the number of accessible active sites and matrix integration, hence improving the overall catalytic activity. In theory, reducing the particle size should at some stage result in an optimized OER activity. However, OER activity optimization as a function of the particle size is not commonly reported in literature[26]. The lack of focus in literature is perhaps derivative of the still ambiguous nature of the material's activity. Different theories are being published in attempts to prove the nature of catalytically active sites and the nature of NiFe LDH's OER activity through time[27,28]. This work aims to present a systematic study as to the extent to which particle size can be used to enhance the catalytic abilities of NiFe LDH and morphologically similar catalysts for oxygen evolution by water electrolysis. Additionally, the compatibility of the size-controlled material of NiFe LDH with composite additives will be investigated for even higher OER activity. Carbon materials such as CNT[20,21], graphene[29–31], and graphene oxides (GO)[19,32] are often

[1]School of Chemistry, Trinity College Dublin, Dublin, Ireland. [2]CRANN & AMBER, Trinity College Dublin, Dublin, Ireland. [3]School of Physics, Trinity College Dublin, Dublin, Ireland. [4]CENIMAT|i3N Departamento de Ciência de Materias, Faculdade de Ciências e Tecnologia, Universidade NOVA de Lisboa and CEMOP/UNINOVA, Campus da Caparica, Portugal. [5]Faculty of Electrical Engineering and Information Technology, Universität der Bundeswehr München, Neubiberg, Germany. [6]I-Form research, Trinity College Dublin, Dublin, Ireland. ✉email: nicolov@tcd.ie

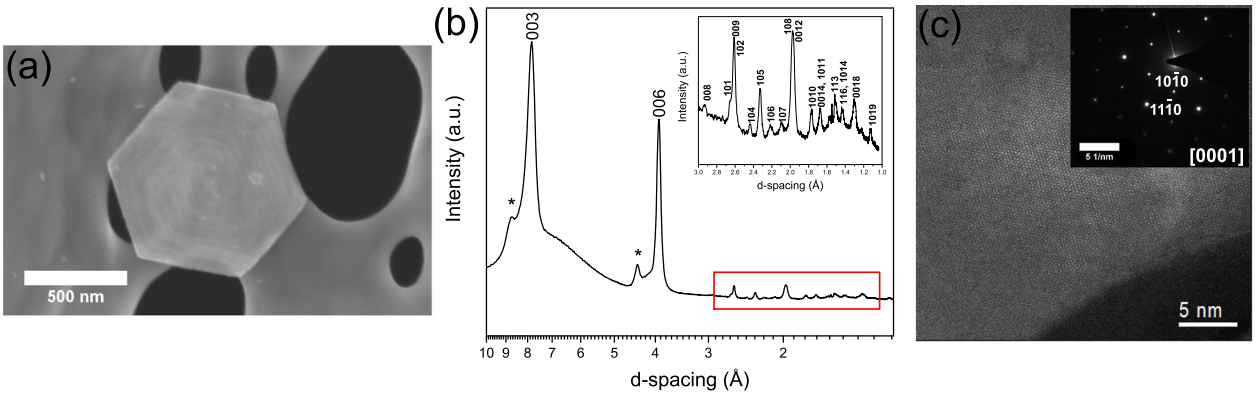


**Fig. 1 Structural characterization of NiFe LDH hexagonal platelets. a** SEM micrograph, **b** Mo Kα-source XRD diffraction pattern (inset, zoomed signals for the 1.3-3 Å d-spacing region), **c** atomic-resolution HAADF-STEM (inset, SAED pattern) for as-synthesized NiFe LDH. Scale bars are **a** 500 nm, **c** 5 nm and inset, 5 1/nm.

considered as desirable components in electrocatalyst composite materials due to their high conductivity and impressive mechanical properties. However, it is important to consider that carbon materials may corrode significantly at high potentials and are also known to contain impurities, including Ni and Fe, which may act as sites for OER. Such considerations are held in regard in this work when testing carbon composite catalysts. In this work, single-wall carbon nanotubes (SWCNT) are investigated due to their strong, flexible, lightweight nature, which makes them potentially the most compatible additive for the size reduced (sr)-NiFe LDH platelets. Ultimately, identifying an appropriate composite system should produce a somewhat optimized catalyst of the material with competitive OER behavior.

## RESULTS AND DISCUSSION

### Synthesis and characterization of NiFe LDH platelets

NiFe LDH was synthesized by way of homogeneous coprecipitation of $Ni^{2+}$ and $Fe^{3+}$ and using a triethanolamine (TEA) capping agent. This synthetic route has been shown to yield pure, highly crystalline NiFe LDH hexagonal platelets with planar morphology[17], as shown in Fig. 1a. The platelets exhibit sharp edges and relatively homogeneous surface, with some patches indicating the presence of minor amounts of residual TEA, on the surface, which have accumulated during preparation[17]. The sharp hexagonal features and regular planar morphology have significance here because they are qualities which have been shown to improve catalytic performance for the OER relative to other morphologies, which may result from different synthetic routes[17]. Combined quantitative compositional thermogravimentric analysis (Supplementary Fig. 1) and atomic absorption spectroscopy approaches give an estimated molecular formula $Ni_{0.78}Fe_{0.22}(OH_2)(CO_3)_{0.11}$-$0.5H_2O$. The X-ray diffraction (XRD) pattern shown in Fig. 1b was indexed as hexagonal symmetry with lattice parameters a = 3.08 Å, c = 23.55 Å. The high-intensity peaks in the diffractogram such as (003) represent high-symmetry directions within the crystal and suggest a highly crystalline nature of the sample[24]. The accurate peak matching also suggests that the sample is pure. The lattice parameters are consistent with the 7.8 Å interlayer spacing expected between layers of $CO_3^{2-}$ intercalated NiFe LDH[33]. Two unmatched peaks (labeled * in Fig. 1b) suggest the presence of some minor swollen phase relative to the dominant $CO_3^{2-}$ intercalated material. It is known that some residual TEA is present within the synthesized material, as evidenced by Jaskaniec et al.[17], characterized with infrared spectroscopy. Given the otherwise high degree of purity, it is reasonable to suggest that TEA intercalation is responsible for the minor phase. Additional atomic-resolution HAADF-STEM imaging (Fig. 1c) indicates a defect-free, crystalline surface, while the hexagonal orientation of the bright SAED pattern (inset) is characteristic of the symmetry within a highly ordered LDH structure[24]. Coupling this with XRD data, the first two families of bright spots can be indexed as (10-10) and (11-10) directions. These results confirm that the used synthesis route maximizes the product's crystallinity and morphological regularity for this synthetic approach. NiFe LDH platelets produced as such can significantly enhance the OER activity of a nickel foam catalyst when the material is homogeneously deposited on the surface (Supplementary Fig. 2).

### Mechanical size-reduction of NiFe LDH platelets

SEM micrographs (Fig. 2a) over an extended sample area, reveal that well-defined hexagonal platelets have been formed throughout with a high degree of regularity in terms of platelet morphology and size. A particle size study was carried out by measuring individual particle lateral dimensions within a sample set between adjacent corners (Fig. 2b and Supplementary Methods). This study revealed that as-produced hexagons had an average lateral length 0.78 ± 0.2 µm, with the majority of the flakes existing in a relatively narrow size range of 0.4–1 µm. This is consistent with submicron NiFe LDH lateral dimensions reported in the literature (smaller than most LDH species), which is known to be one of the materials' significant features in terms of electrochemical activity[24]. Ultrasonication of the as-produced platelets using a tip-sonication method can be used to further reduce the average particle size. When high power tip sonication is applied, the shear stress required for exfoliation can be surpassed and out-of-plane particle breaking dominates. In this way, fragmentation of the LDH platelets can be achieved, resulting in average particle size reduction. Figure 2c and d reveal that the original NiFe LDH hexagons can be reduced to platelets of 0.29 ± 0.01 µm. Comprehensively characterizing the material in terms of crystallinity, composition, and chemical state before and after the size reduction step, it can be demonstrated with some certainty that the processing to this point has no effect of any significance aside from platelet fracturing (Supplementary Figs. 3–5). The only effect is morphological, with the material retaining crystalline and compositional homogeneity across the platelets and, importantly, at newly exposed edge sites. This can rule out the possibility of preferential breaking directions or effects like the dissolution of components upon fragmentation, which would likely bring about some shift in the local crystalline structure. Additionally, an introduction of surface defects, which could effect the activity across exposed basal planes, is undetectable using Ni $2p_{3/2}$ XPS surveys.

Synthetic approaches to platelet size control have been previously demonstrated for LDH compounds. For example, Xu et al.[34], demonstrated synthetic size control of MgAl LDH by subtly

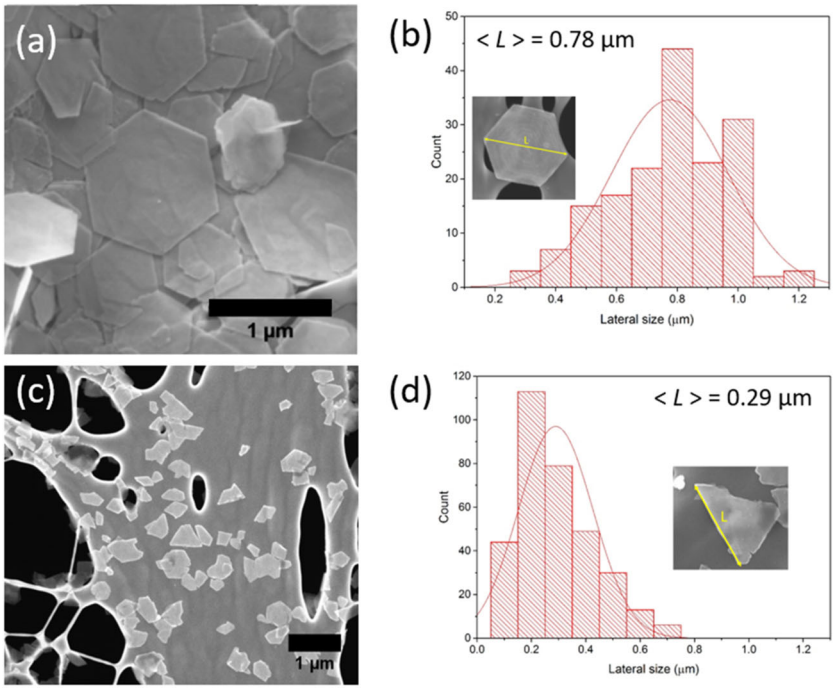


**Fig. 2 Demonstration of platelet size reduction upon sonication treatment. a** and **c** SEM micrographs of as-produced and size-reduced platelets respectively and **b** and **d** associated platelet size distributions indicating mean platelet size. (Inset (**b** and **d**) indicate the method of measuring lateral platelets size L). Scale bars are 1 μm in (**a** and **c**).

changing parameters, such as hydrothermal treatment time and temperature during synthesis. However, many chemical properties are nontransferable when one switches between LDH compounds with different metal-center combinations. This is the case here as similar synthetic size control techniques could not be replicated for the $Ni^{2+}$ and $Fe^{3+}$ combination. The non-amphoteric nature of $Fe^{3+}$ intermediates in the coprecipitation reaction scheme is likely the critical factor[33,35,36]. Controlled average particle size for colloidal dispersions can be achieved using centrifugation to produce a range of unique particle dispersions whose mean flake length (<*L*>) varies in a sequential manner (Supplementary Fig. 6).[37] The process involves carefully choosing centrifugation conditions (time and rate in rotations per minute (rpm)), which will apply enough centrifugal force to the colloids to cause sedimentation of some but not all of the dispersion. What is left after a successful centrifugation step is a dispersed "supernatant" (smaller <*L*>) and sediments (larger <*L*>). In this work, a combination of fragmentation and centrifugation steps were used to produce three particle dispersions each with a unique size distribution (Fig. 3a–f) prepared from a range of 500 to 7000 rpm. The upper centrifugation limit was set at 7000 rpm for this work to ensure contamination from foreign particles did not become a factor when attempting to achieve accurate mass loading. Within this range, it is possible to attain unique size distributions (i.e. average lateral particle size <*L*>), albeit with some overlap of standard deviations ($\sigma$). Nevertheless, polarization curves (Fig. 3j) indicate a significant overpotential reduction (at 10 $mA.cm^{-2}$) for particles centrifuged at 7000 rpm. It is not always possible to observe an obvious trend in the quoted overpotentials, so it is useful to cycle the LDH electrodes using cyclic voltammetry (CV) within a fixed potential range (3g–i), which should allow the materials to stabilize to some extent[15,38]. This should provide a more realistic set of overpotential values for comparing electrode performances (Fig. 3k). For each sample, the redox activity just below the onset potential for catalysis is consistent with the behavior of the as-synthesized NiFe LDH hexagons deposited on Ni foam (Supplementary Fig. 2c) and consist of $Ni^{2+}/Ni^{3+}$ redox couples in different compositional and structural environments, with subtle phase transitions being induced during early cycling to cause peak shift and splitting. Additionally, the gradual growth of surface hydrous oxides on the catalyst with cycling gives the appearance of current enhancement for the respective peaks (see Supplementary Note for full details). Vitally, the effects are consistent across size-selected samples and as such cannot be judged to influence the catalytic improvement for smaller platelets. In addition, there were no changes of significance in the AFM surface profiles or zeta potentials for the size-selected material (Supplementary Fig. 7), meaning there can be no serious influence of surface charge or surface roughness on the relative performances. Thus, the enhancement of respective size-selected platelets is judged as an effect of their relative density of active edge sites. During early cycling one can see the overpotential fluctuating quite rapidly, reaching overpotentials more than 50 mV below initial discharge values. In this time, it is thought that a combination of subtle crystallographic phase changes and active-site degradation produce the unique shape. Phase changes have been observed for nickel-hydroxide-based OER catalysts in alkaline media. The transitions involve an initial hydrated $\alpha$-hydroxide phase which can contract to a $\gamma$-oxyhydroxide phase upon $Ni^{2+}$ oxidation (along with deprotonation of interlamellar $H_2O$), and further to a significantly denser, dehydrated $\beta$-hydroxide/oxyhydroxide crystal, as described by Bode et al.[39] More recently, Dionigi et al.[28] have demonstrated analogous phase changes within NiFe mixed-metal catalysts. It is in fact possible to detect contractions in the basal plane after cycling by way of postmortem XRD analysis (Supplementary Fig. 8), which aligns precisely with the expected dimensions of the $\gamma$-hydroxide phase, based on the analogy with the Bode cycle. This is the extent of phase transitions for NiFe LDH catalysis, as Trotochaud et al.[38] demonstrate for $Ni(OH)_2$, with any significant Fe inclusion the crystal does not produce a structural $\beta$-phase. The $\alpha \rightarrow \gamma$ transition generally takes place during early cycling and allows for some improvement in electrochemical performance (i.e. lower overpotentials in this case). Although the principle degradation effects

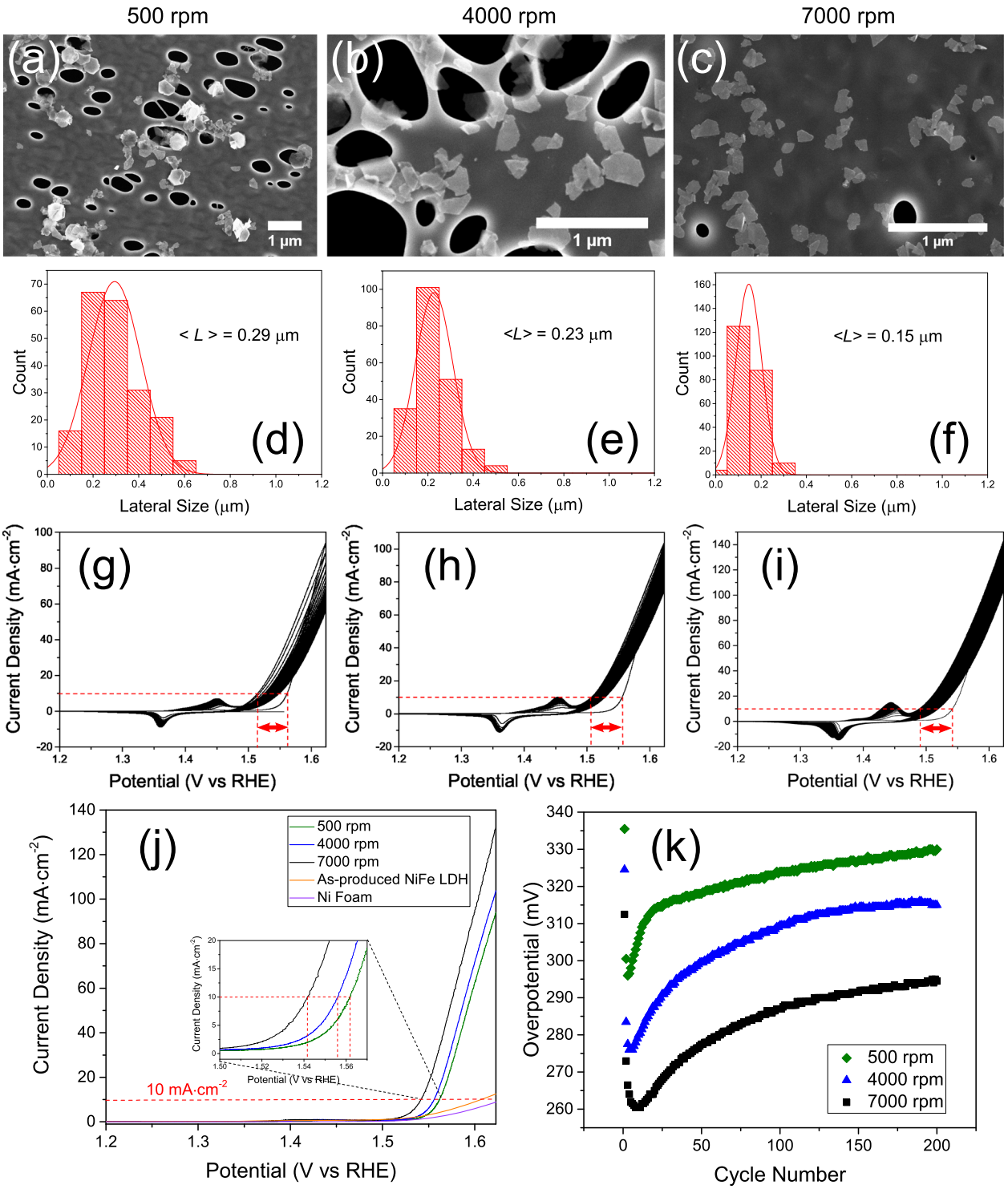


**Fig. 3 Summary of the relationship between controlled platelet sizes and electrocatalytic output. a**–**c** SEM micrographs and **d**–**f** accompanying size-distribution histograms for the sr-NiFe LDH with final centrifugation rates 500, 4000, and 7000 rpm, respectively. **g**–**i** CVs over 200 cycles for each of the respective electrodes. Quoting the anodic potentials at 10 mA.cm$^{-2}$ of successive cycles allowed the overpotentials to be tracked during an extended catalyst lifetime. **j** Initial polarization curves for electrodes prepared with each dispersion and **k** overpotentials as a function of cycle number, averaged over two-electrode samples in each case (full data in Supplementary Fig. 9a). Scale bars are 1 μm in (**a**, **b**, and **c**).

causing the subsequent sharp rise in $\eta$ from cycle number four onward is not exactly known, it is likely a result of the leaching of some metal centers from the catalyst crystal structure in response to OER activity over time. Beyond this, the $\eta$ values approach equilibrium for the three samples and one can start to see an apparent correlation between the overpotentials and the final centrifugation rate (and hence <*L*>). This is a subtle difference between samples but provides a proof-of-concept representation of the proposed theory, which is also reflected in cell stability tests over extended time periods (Supplementary Fig. 9b).

Electrochemical surface area (ECSA) analysis complements the observation as it shows no detectable increase in active surface area for size-reduced material (Supplementary Fig. 10). This points toward active edge sites rather than basal plane activity as the principal area. Additionally, the process is highly reproducible over different particle size distributions. Supplementary Fig. 11 represents an example of the same principle size-activity relationship but over a broader range of <*L*>. With values as low as 245 ± 7 mV at 10 mA.cm$^{-2}$ current density (before iR-correction), the sr-NiFe LDH material prepared here represents a significant improvement on reported pure materials in the literature (Table 1). For example, Jaskaniec et al.[17] report 340 mV at 10 mA.cm$^{-2}$, while Diaz-Morales et al.[40] report 290 mV at just 1 mA.cm$^{-2}$. In fact, the majority of literature values are reported around 300 mV for pure NiFe LDH.[9,24] Efforts now must be made to retain the impressive catalysis of the sr-NiFe beyond its early cycle life. The performance of composites of this nature is heavily influenced not only by the intrinsic properties of the components but also by their interfacial connectivity, and hence the method of preparation. In this sense parameters like overpotential and Tafel slope (Table 1) can give a good indication of a catalyst system's worth, but it is important to remember that there are a number of additional factors such as current density, mass loading, and choice of substrate and electrolyte, which can also influence the results[41,42]. Thus, in the following section, the effect of carbon nanotube matrices on the extended activity of sr-NiFe LDH platelets will be presented.

**Table 1.** Comparative OER activities for various competitive NiFe LDH catalyst systems (* this work).

| Catalyst | $\eta$ @ 10 mA.cm$^{-2}$ (mV vs RHE) | Current density (mA. cm$^{-2}$) | Tafel slope (mV.dec$^{-1}$) | Mass loading (mg. cm$^{-2}$) | Substrate |
|---|---|---|---|---|---|
| $IrO_2$[24] | 338 | 10 | 47 | 0.21 | GC |
| NiFe LDH[17] | 360 | 5 | n/a | 0.12 | NF |
| NiFe Nanosheets[24] | 302 | 9.4 | 40 | 0.07 | GC |
| NiFe-CNT[25] | 220 | 10 | 31 | 0.25 | GC |
| NiFe-rGO[31] | 230 | 10 | 42 | 0.25 | GC |
| NiFe@NiCoP[5] | 220 | 10 | 49 | 2 | NF |
| **sr-NiFe*** | 245 | 10 | 32 | 0.16 | NF |
| **sr-NiFe-CNT*** | 237 | 10 | 32 | 0.16 | NF |

## NiFe LDH-SWCNT nanocomposite

In the interest of improving cyclability and combating the $\eta$ losses, composite studies are carried out in addition to size treatment, the aim being to minimize overlap of adjacent NiFe LDH platelets, while providing an integrated conductive matrix, which can facilitate the rapid electrochemical mechanism. A number of interesting composite materials have been suggested and researched for LDH-based OER catalysis in recent times including various carbon allotropes[32,43], metal-organic frameworks (MOF)[29,44], and more novel materials, often various nanowires[45,46]. However, CNTs have most notably been demonstrated as useful additives to this end, yielding improved overpotential, Tafel slope, conductivity, and stability when coupled with NiFe LDH in alkaline electrolyzer systems. CNTs represent a well-established option as a conductive additive in electrochemistry, while also being readily available. Composites of the sr-NiFe LDH and SWCNT materials were made by mixing IPA dispersions of each. In order to attain a well-integrated composite system, good connectivity needed to be achieved. However, the affinity between LDHs and SWCNT proved to be weak. Some relatively low-power tip sonication after mixing can help achieve higher connectivity within the LDH-SWCNT matrix, which is reflected electrochemically (Supplementary Fig. 13). Using this approach, composites of different SWCNT weight percentages were prepared and compared by cycling 50 times under OER conditions.

According to Fig. 4a, it can be noted then that SWCNT additives may act to minimize inter-particle contact of sr-NiFe LDH particles within the OER electrode as well as providing the expected conductive matrix. Not surprisingly, this system leads to improved retention of the overpotential values beyond four to five cycles (Fig. 4b). While trace amounts of Ni and Fe are detectable within the SWCNTs (Supplementary Fig. 14), control experiments involving cycling pure SWCNTs on Ni foam indicate that no significant contribution is made to the OER (Supplementary Fig. 15). Although mass loading was previously optimized as 0.12 mg. cm$^{-2}$ for pure NiFe LDH electrodes, replacing some percentage of the mass with a foreign species will likely affect this. Mass loading in the range 0.12–0.18 mg.cm$^{-2}$ was tested for samples containing 10, 15, and 20 weight % of SWCNT with NiFe LDH. If the mass loading is kept consistent across samples of various SWCNT wt% an inverse relationship is observed, with the electrocatalytic output decreasing (higher $\eta$ values) with more SWCNT (Fig. 4b). This is expected as there would be fewer active components in each case. This can be compensated by increasing the mass loading to a particular value for each composite. The ideal loading in each case (Fig. 4c) demonstrated similar electrocatalytic behavior. Mass loading was optimized by trial.

Combining size-controlled platelets in composite systems, fully optimized electrodes were prepared by mixing sr-LDH (0.16 ± 0.0 µm, 5000 rpm) in IPA with 20 wt% SWCNT, followed by composite spraying on nickel foam to 0.17 mg.cm$^{-2}$ mass loading. The final product gives an impressive electrocatalytic output with

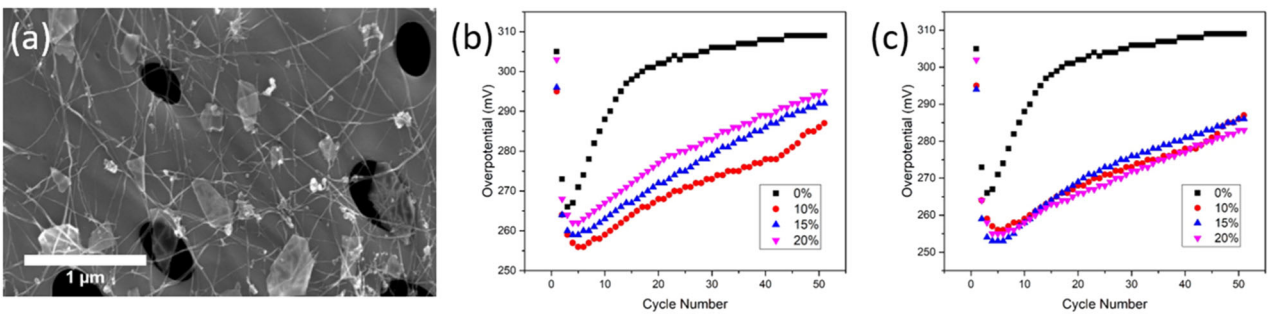


**Fig. 4 Optimization of integrated composite materials. a** SEM of sr-NiFe-SWCNT composite on lacey carbon and **b** comparison of overpotentials through 50 cycles of OER electrodes prepared using sr-NiFe with 10, 15, and 20 weight % SWCNT with identical mass loading and **c** optimized mass loading. Scale bar is 1 µm in **a**.

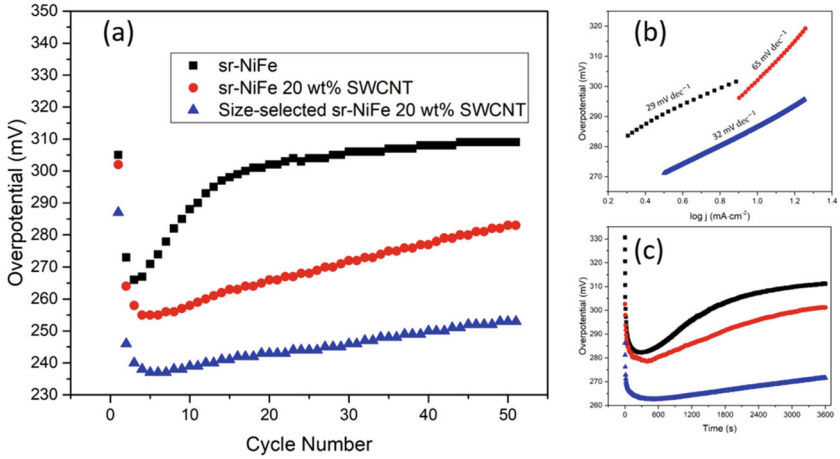


**Fig. 5 Performance summary for 'fully optimized' catalysts in the scope of this work.** Comparison of **a** overpotentials through 50 cycles and **b** Tafel slopes of OER electrodes prepared using size-selected sr-NiFe LDH with 20 wt% SWCNT, a nonsize-selected composite and pure sr-NiFe LDH. **c** Chronopotentiometry curve of the optimized electrode through 1 h at 10 mA.cm$^{-2}$.

an overpotential reading of 237 ± 7 mV vs RHE, which, within the calculated uncertainty for $\eta$ values, shows little improvement on the pure size-selected sr-NiFe LDH particles. The real improvement in the composite becomes clear with cycling, as the retention through 50 cycles is the highest yet, with just 7% increase in $\eta$ (Fig. 5a), a considerable long-term improvement on what could be demonstrated with the treated LDH material alone.

Upon further cycling, a stable value is reached at around 275 mV (Supplementary Fig. 16). By studying Tafel slopes (Fig. 5b) one can gain some insight into the improved electrocatalysis of the optimized electrode. Graphs of this kind are based on the Tafel equation (Eq. (2)), which relates the overpotential $\eta$ to the current density $j$ (and exchange current density $j_0$) so that the proportionality constant $b$ (Tafel slope) will give information regarding the sensitivity of the reaction rate to a change in potential across the cell:

$$\eta = b \times \log_{10} \frac{j}{j_0} \tag{1}$$

The increase in $b$ upon initial introduction of carbon additives suggests the sensitivity is inhibited but once particle size selection is applied, the value returns almost to that of the pure sr-NiFe. With considerable particle size reduction within a given electrode, an increase in the contact area between the active material and conductive SWCNT matrix is achieved which is likely allowing for this positive effect on the Tafel slope. This in turn suggests improved kinetics within the optimized electrode which will have a positive effect in electrochemistry. Chronopotentiometry (Fig. 5c) represents a more practical test of performance for an electrolyzer cell with no cycling, but rather an overpotential gradient when subjected to constant current density. After 1 h, the overpotential value remains below 280 mV with a relatively shallow slope and remains below 295 mV after 12h (Supplementary Fig. 17). This performance suggests improvement over similar NiFe LDH-carbon-based composite materials in the field of OER catalysis[5,25,31]. Further stability testing on timescales of one week (Supplementary Fig. 18) demonstrate the continued activity with overpotentials remaining below 360 mV, despite some apparent fluctuations caused by large bubbles forming on the surface of the active catalyst in the presented static setup. It is thought that at these extended timescales, the catalytic stability is governed by a number of possible factors, including continued leaching of the metal components from the structure and the growth of a surface hydrous oxide layer. In conclusion, combined postsynthesis processing techniques of size selection and composite preparation have been combined to improve the electrocatalytic outlook for NiFe LDH material as a highly active nonprecious metal-based anode in an alkaline electrolyzer cell. This presents a low-cost, scalable, and low-energy process from chemical synthesis to device preparation. The electrodes were tested with the aim of determining their practical viability in operating conditions by predominantly studying cycle life rather than conventional polarization curves to understand the processes which dominate the catalytic output in the early cycle life of an electrolyzer cell. Additionally, this work suggests, from an electrochemical perspective, the existence of a majority of catalytically active sites around platelet edges with a minority along the planar surface based on the effect observed of decreasing the mean platelet sizes $\langle L \rangle$ on overpotentials achieved. Overall, this study aimed to utilize this effect to offer a simple yet effective set of steps that allow notable improvements in the catalytic behavior of electrochemically active platelet-like materials, which is not limited to the combination of metals considered here.

In conclusion to the presented work, highly crystalline NiFe LDH planar hexagons with mean lateral dimensions 0.78 ± 0.2 µm were synthesized by homogeneous precipitation and studied based on their OER electrocatalytic properties and the potential for enhancement by particle size control. Postsynthetic treatment of the material involved centrifugation-driven size selection and particle breaking using tip sonication. The treatment methods were shown to be successful by various characterization techniques and improved the OER overpotential relative to the as-produced material. The extent to which centrifugation could be used as a size-selection tool for platelets in the range 0.2–1.2 µm was encouraging. It was possible to selectively isolate platelet dispersions with a mean flake size as small as $\langle L \rangle = 0.15 \pm 0.01$ µm by centrigugation with superior overpotential compared to the bulk NiFe LDH. As well as that, size-selected samples demonstrate a direct relationship that exists between the size and catalytic behavior. This assumption carries through in the electrochemical data at very least, with the broken particles (from tip sonication combined with centrifugal size selection), providing the best OER overpotential within the framework of this project, $\eta = 245 \pm 7$ mV ($\langle L \rangle = 0.2 \pm 0.01$ µm). The intrinsic redox behavior and structural phase transitions, which occur within the LDH crystals during the extended catalyst lifetime are tracked and accounted for across all platelet sizes and cannot be deemed to influence the respective performance. There is still room for progress in terms of preparing electrochemical cells which can emulate the most competitive overpotentials reported in the literature to date. For instance, catalysts based on NiFe LDH composites were studied as well for their catalytic enhancement properties. Composites based on

carbon nanotubes increased the electron transport capability of the material. The results suggest that a well-connected system can be achieved between the active component and carbon additive without the necessity of a bottom-up approach, involving direct growth onto a carbon network. In fact, sr-NiFe LDH appears quite compatible in composite systems with SWCNTs in weight ratios of 10–20%. Composites prepared as such for this work ($<L> = 0.16 \pm 0.005$ µm, 20 wt% SWCNT) displayed excellent cycling performance compared with the active material alone, capable of lower stable overpotentials beyond 150 cycles. Further OER enhancement may result from achieving complete homogeneous deposition of NiFe LDH platelets onto Ni foam substrates with mass loading between 0.1 and 0.2 $mg.cm^{-2}$ and without agglomeration. This was achieved by using ultrasonic tip spraying. This should allow more complete deposition of the active material across the entire electrode surface and so produce more competitive overpotential values in relation to ongoing research in the field of OER catalysis.

## METHODS

### NiFe LDH synthesis

$Ni(NO_3)_2.H_2O$, $Fe(NO_3)_3.9H_2O$, urea, and triethanolamine (TEA) were made into a 200 mL solution using deionized (DI) water such that their respective concentrations were 7.5 mM, 2.5 mM, 17.5 mM, and 10 mM, respectively. The resulting solutions were stirred at 150 rotations per minute (rpm) at room temperature for 24 h, after which a brown precipitate was observed. Next, the reaction mixture was split into two 100 mL round bottom flasks (80 mL in each) and heated under reflux to 100 °C in an oil bath for 48 h. Afterward the system was allowed to cool naturally to room temperature. The obtained dispersion was then centrifuged at 3000 rpm for 10 min to precipitate the NiFe LDH platelets. The prepared material was then washed three times by dispersing the sediments in DI water by shaking, followed by centrifugation (5000 rpm for 10 min using a Heraeus Multifuge XI Centrifuge). The clean powders were then washed similarly in IPA before re-dispersing and storing for further use. All chemicals were purchased from Sigma-Aldrich and used without any modification.

### NiFe LDH characterization

The clean material powders dispersed in IPA were then characterized by means of SEM, TEM, XRD, and SAED to determine chemical composition, crystallinity, and morphology. SEM was carried out using a Zeiss Ultra Plus field-emission microscope with a Gemini column and a secondary-electron detector, operating in accelerating voltage range 2–5 keV. TEM images were taken using an FEI Titan 80–300 kV FEG STEM microscope with SAED acquired in-situ in this machine. Powder XRD was carried out using a Bruker Advance Powder X-ray diffractometer with a molybdenum K-$\alpha$ emission source in the Bragg-Brentano configuration. XPS measurements were performed using an Omicron XPS model EA125 with a monochromatic Al K$\alpha$ source, where the binding energy was calibrated to the C 1s peak.

### Centrifugal size-selection

Sample dispersion of NiFe LDH in IPA was size selected by initially centrifuging at 500 rpm using a Heraeus Multifuge X1 Centrifuge with a F15-6x100y carbon fiber rotor.

### Electrodes manufacturing

The electrodes for OER testing were prepared by spraying NiFe LDH component onto a nickel foam using a USI Prism Ultracoat 300 spray tool with the substrate kept at 100 °C. A flow rate of 0.5 mL/min was used and mass loading was monitored using a Sartorius SE2 ultramicrobalance.

### SWCNT dispersions preparation

Dispersions of SWCNTs in IPA were prepared by adding 10 mg of SWCNT powder (P3-SWCNT, Carbon Solutions Inc. - Supplementary Fig. 14) to 100 mL of IPA and applying ultrasonication by way of tip sonication (Fischer Scientific Sonic Dismembrator Ultrasonic Processor) at 40% power for 45 min assisted by a cooling system maintaining the dispersion at 5 °C. Following that, bath sonication at 37 kHz was applied to the dispersion for 1 h using a Fisherbrand 112xx Series Advanced Ultrasonic Cleaner at 60% power.

### Composite preparation

Composites were prepared using known concentrations of SWCNT and NiFe LDH suspensions in isopropanol (IPA). Appropriate volumes of each were measured out using glass pipettes in order to achieve 10 mL samples of 10, 15, and 20 weight% SWCNT wrt NiFe LDH. In order to achieve good contact between the components, further tip sonication at 40% power for 10 min was applied.

### Electrochemical testing

The electrodes were placed in a three-electrode setup with a platinum wire acting as the counter and Ag/AgCl reference electrode (3.5M KCl-filling solution). The electrolyte used was 1M potassium hydroxide (KOH) solution. Cyclic voltammetry, linear voltammetry and chronopotentiometry were utilized as the principle characterization tools in terms of electrochemistry. The potentiostat used was a BioLogic VMP 300. Voltage sweep rates were kept at 5 $mV.s^{-1}$ in a potential window 0–0.6 V (vs Ag/AgCl) for all voltamograms. The potential measured vs Ag/AgCl is mathematically converted to potential vs reversible hydrogen electrode (RHE) according to Eq. (2):

$$E_{RHE} = E_{Ag/AgCl} + 0.059 \cdot pH + E^0_{Ag/AgCl} \quad (2)$$

where $E^0_{Ag/AgCl}$ is the saturated Ag/AgCl electrode potential equal to 0.197 V at 25 °C.

## DATA AVAILABILITY

The data relating to the findings of this work is available from the corresponding author, subject to reasonable request.

Received: 30 November 2020; Accepted: 25 June 2021;
Published online: 11 August 2021

## REFERENCES

1. Yang, R. et al. Synergistic coupling of CoFe-LDH arrays with NiFe-LDH nanosheet for highly efficient overall water splitting in alkaline media. *Appl. Catal. B.* **253**, 131–139 (2019).
2. Zhong, H. et al. Template-free synthesis of three-dimensional NiFe-LDH hollow microsphere with enhanced OER performance in alkaline media. *J. Energy Chem.* **33**, 130–137 (2019).
3. Nikolaidis, P. & Poullikkas, A. A comparative overview of hydrogen production processes. *Renew. Sust. Energ. Rev.* **67**, 597–611 (2017).
4. Dong, Y. et al. Structural instability induced high-performance NiFe layered double hydroxides as oxygen evolution reaction catalysts for pH-near-neutral borate electrolyte: the role of intercalates. *Appl. Catal. B.* **263**, 118343 (2020).
5. He, J. et al. Structure-property relationship of graphene coupled metal (Ni, Co, Fe) (oxy)hydroxides for efficient electrochemical evolution of oxygen. *J. Catal.* **377**, 619–628 (2019).
6. Doyle, R. L. & Lyons, M. E. *Photoelectrochemical solar fuel production*, 41–104 (Springer, 2016).
7. Koper, M. T. Thermodynamic theory of multi-electron transfer reactions: implications for electrocatalysis. *J. Electroanal. Chem.* **660**, 254–260 (2011).
8. Hunter, B. M., Winkler, J. R. & Gray, H. B. Iron is the active site in nickel/iron water oxidation electrocatalysts. *Molecules.* **23**, 903 (2018).
9. Tahir, M. et al. Electrocatalytic oxygen evolution reaction for energy conversion and storage: a comprehensive review. *Nano Energy.* **37**, 136–157 (2017).
10. Suen, N. T. et al. Electrocatalysis for the oxygen evolution reaction: recent development and future perspectives. *Chem. Soc. Rev.* **46**, 337–365 (2017).
11. Lu, Z. et al. Three-dimensional NiFe layered double hydroxide film for high-efficiency oxygen evolution reaction. *Chem. Commun.* **50**, 6479–6482 (2014).
12. Dionigi, F. & Strasser, P. Nife-based (oxy) hydroxide catalysts for oxygen evolution reaction in non-acidic electrolytes. *Adv. Energy Mater.* **6**, 1600621 (2016).
13. Cai, X. et al. Solvothermal synthesis of NiCo-layered double hydroxide nanosheets decorated on RGO sheets for high performance supercapacitor. *Chem. Eng. J.* **268**, 251–259 (2015).
14. Li, J., Jiang, S., Shao, M. & Wei, M. Host-guest engineering of layered double hydroxides towards efficient oxygen evolution reaction: recent advances and perspectives. *Catalysts.* **8**, 214 (2018).
15. Bandal, H., Reddy, K. K., Chaugule, A. & Kim, H. Iron-based heterogeneous catalysts for oxygen evolution reaction; change in perspective from activity promoter to active catalyst. *J. Power Sources.* **395**, 106–127 (2018).

16. Delgado, D., Bizzotto, F., Zana, A. & Arenz, M. Accelerated durability test for high-surface-area oxyhydroxide nickel supported on raney nickel as catalyst for the alkaline oxygen evolution reaction. *ChemPhysChem.* **20**, 3147–3153 (2019).
17. Jaśkaniec, S. et al. Low-temperature synthesis and investigation into the formation mechanism of high quality Ni-Fe layered double hydroxides hexagonal platelets. *Sci. Rep.* **8**, 4179 (2018).
18. Li, X., Hao, X., Wang, Z., Abudula, A. & Guan, G. In-situ intercalation of NiFe LDH materials: an efficient approach to improve electrocatalytic activity and stability for water splitting. *J. Power Sources.* **347**, 193–200 (2017).
19. Zhan, T., Liu, X., Lu, S. S. & Hou, W. Nitrogen doped NiFe layered double hydroxide/reduced graphene oxide mesoporous nanosphere as an effective bifunctional electrocatalyst for oxygen reduction and evolution reactions. *Appl. Catal. B.* **205**, 551–558 (2017).
20. Chen, R. et al. Achieving stable and efficient water oxidation by incorporating NiFe layered double hydroxide nanoparticles into aligned carbon nanotubes. *Nanoscale Horiz.* **1**, 156–160 (2016).
21. Liu, H. et al. Integrated flexible electrode for oxygen evolution reaction: layered double hydroxide coupled with single-walled carbon nanotubes film. *ACS Sustain. Chem. Eng.* **6**, 2911–2915 (2018).
22. Zhou, D. et al. Effects of redox-active interlayer anions on the oxygen evolution reactivity of NiFe-layered double hydroxide nanosheets. *Nano Res.* **11**, 1358–1368 (2018).
23. Zhang, L. et al. Facilitating active species generation by amorphous NiFe-Bi layer formation on NiFe-LDH nanoarray for efficient electrocatalytic oxygen evolution at alkaline pH. *Chem. Eur.* **23**, 11499–11503 (2017).
24. Song, F. & Hu, X. Exfoliation of layered double hydroxides for enhanced oxygen evolution catalysis. *Nat. Commun.* **5**, 1–9 (2014).
25. Gong, M. et al. An advanced ni–fe layered double hydroxide electrocatalyst for water oxidation. *J. Am. Chem. Soc.* **135**, 8452–8455 (2013).
26. McAteer, D. et al. Liquid exfoliated Co(OH) 2 nanosheets as low-cost, yet high-performance, catalysts for the oxygen evolution reaction. *Adv. Energy Mater.* **8**, 1702965 (2018).
27. Chen, R. et al. Layered structure causes bulk nife layered double hydroxide unstable in alkaline oxygen evolution reaction. *Adv. Mater.* **31**, 1903909 (2019).
28. Dionigi, F. et al. In-situ structure and catalytic mechanism of nife and cofe layered double hydroxides during oxygen evolution. *Nat. Commun.* **11**, 1–10 (2020).
29. Tang, C. et al. Spatially confined hybridization of nanometer-sized NiFe hydroxides into nitrogen-doped graphene frameworks leading to superior oxygen evolution reactivity. *Adv. Mater.* **27**, 4516–4522 (2015).
30. Feng, Y., Zhang, H., Zhang, Y., Li, X. & Wang, Y. Ultrathin two-dimensional free-standing sandwiched NiFe/C for high-efficiency oxygen evolution reaction. *ACS Appl. Mater. Interfaces.* **7**, 9203–9210 (2015).
31. Ma, W. et al. A superlattice of alternately stacked ni–fe hydroxide nanosheets and graphene for efficient splitting of water. *ACS Nano.* **9**, 1977–1984 (2015).
32. Youn, D. H. et al. One-pot synthesis of NiFe layered double hydroxide/reduced graphene oxide composite as an efficient electrocatalyst for electrochemical and photoelectrochemical water oxidation. *J. Power Sources.* **294**, 437–443 (2015).
33. Abellán, G., Coronado, E., Martí-Gastaldo, C., Pinilla-Cienfuegos, E. & Ribera, A. Hexagonal nanosheets from the exfoliation of Ni2+-Fe 3+ LDHs: a route towards layered multifunctional materials. *J. Mater. Chem.* **20**, 7451–7455 (2010).
34. Xu, Z. P., Stevenson, G., Lu, C.-Q. & Lu, G. Q. Dispersion and size control of layered double hydroxide nanoparticles in aqueous solutions. *J. Phys. Chem.* **110**, 16923–16929 (2006).
35. Ma, R. et al. Synthesis and exfoliation of co2+- fe3+ layered double hydroxides: an innovative topochemical approach. *J. Am. Chem. Soc.* **129**, 5257–5263 (2007).
36. Han, Y. et al. Preparation of ni2+- fe3+ layered double hydroxide material with high crystallinity and well-defined hexagonal shapes. *Chem. Mater.* **20**, 360–363 (2008).
37. Khan, U. et al. Size selection of dispersed, exfoliated graphene flakes by controlled centrifugation. *Carbon.* **50**, 470–475 (2012).
38. Trotochaud, L., Young, S. L., Ranney, J. K. & Boettcher, S. W. Nickel–iron oxyhydroxide oxygen-evolution electrocatalysts: the role of intentional and incidental iron incorporation. *J. Am. Chem. Soc.* **136**, 6744–6753 (2014).
39. Bode, H., Dehmelt, K. & Witte, J. Zur kenntnis der nickelhydroxidelektrode-"i. über das nickel (ii)-hydroxidhydrat. *Electrochim. Acta.* **11**, 1079–1087 (1966).
40. Diaz-Morales, O., Ledezma-Yanez, I., Koper, M. T. & Calle-Vallejo, F. Guidelines for the rational design of ni-based double hydroxide electrocatalysts for the oxygen evolution reaction. *ACS Catal.* **5**, 5380–5387 (2015).
41. Garcia, A. C., Touzalin, T., Nieuwland, C., Perini, N. & Koper, M. T. Enhancement of oxygen evolution activity of nickel oxyhydroxide by electrolyte alkali cations. *Angew. Chem. Int. Ed.* **58**, 12999–13003 (2019).
42. Browne, M. P. & Mills, A. Determining the importance of the electrode support and fabrication method during the initial screening process of an active catalyst for the oxygen evolution reaction. *J. Mater. Chem. A* **6**, 14162–14169 (2018).
43. Tang, D. et al. Carbon quantum dot/NiFe layered double-hydroxide composite as a highly efficient electrocatalyst for water oxidation. *ACS Appl. Mater. Interfaces.* **6**, 7918–7925 (2014).
44. Kang, B. K. et al. Mesoporous Ni-Fe oxide multi-composite hollow nanocages for efficient electrocatalytic water oxidation reactions. *J. Mater. Chem.A* **5**, 4320–4324 (2017).
45. Liu, J. et al. Hierarchical NiCo2S4@NiFe LDH heterostructures supported on nickel foam for enhanced overall-water-splitting activity. *ACS Appl. Mater. Interfaces.* **9**, 15364–15372 (2017).
46. Yu, L. et al. Cu nanowires shelled with NiFe layered double hydroxide nanosheets as bifunctional electrocatalysts for overall water splitting. *Energy Environ. Sci.* **10**, 1820 (2017).

## ACKNOWLEDGEMENTS

D.T., S.J., J.C., and V.N. wish to thank the support of the ERC CoG, 3D2DPring (GA 681544) and PoC Powering_eTextiles (GA 861673) and SFI AMBER (12/RC/2278_P2). M. P.B acknowledges the financial support of the European Union's Horizon 2020 Research and innovation program under the Marie Skłodowska-Curie Actions IF under the project TriCat4Energy (Grant Agreement no. 884318). The authors would like to thank the Advanced Microscopy Lab and CRANN Trinity College Dublin for providing STEM-EDX measurements. This publication has emanated from research supported in part by a grant from Science Foundation Ireland under Grant number 12/RC/2278_P2. For the purpose of Open Access, the author has applied a CC BY public copyright licence to any Author Accepted Manuscript version arising from this submission.

## AUTHOR CONTRIBUTIONS

D.T., J.C., M.P.B., S.J., and V.N. took part in discussion and proposal of project structure and planning experiments. Synthesis of NiFe LDH was carried out by D.T. and S.J. SEM was performed by D.T, as well as subsequent analysis of platelet sizes. Electrochemistry was performed by D.T. with assistance from J.C. and M.P.B. TEM analysis was carried out by A.R. along with in-situ EDX mapping and SAED. Diffraction patterns acquired by XRD were performed by B.S. and D.T. XPS surveys were acquired by L.G. and C.M., and fitted by M.P.B. AFM analysis was performed by K.O. and G.S.D. Zeta potentials and TGA measurements were performed by D.T and S.J. Electrochemical data interpretation was carried out by J.C., M.P.B., and D.T. and wider outlook and conclusions were discussed by J.C., M.P.B., S.J., V.N., and D.T. The paper was written by D.T. with assistance from J.C., and all authors contributed to the manuscript.

## COMPETING INTERESTS

The authors declare no competing interests.

## ADDITIONAL INFORMATION

**Supplementary information** The online version contains supplementary material available at https://doi.org/10.1038/s41699-021-00249-6.

**Correspondence** and requests for materials should be addressed to V.N.

**Reprints and permission information** is available at http://www.nature.com/reprints

**Publisher's note** Springer Nature remains neutral with regard to jurisdictional claims in published maps and institutional affiliations.

**Open Access** This article is licensed under a Creative Commons Attribution 4.0 International License, which permits use, sharing, adaptation, distribution and reproduction in any medium or format, as long as you give appropriate credit to the original author(s) and the source, provide a link to the Creative Commons license, and indicate if changes were made. The images or other third party material in this article are included in the article's Creative Commons license, unless indicated otherwise in a credit line to the material. If material is not included in the article's Creative Commons license and your intended use is not permitted by statutory regulation or exceeds the permitted use, you will need to obtain permission directly from the copyright holder. To view a copy of this license, visit http://creativecommons.org/licenses/by/4.0/.

© The Author(s) 2021